Inorganic Chemistry
Article

Inorg. Chem. **2010**, *49*, 695–703 **695**
DOI: 10.1021/ic902005m

Magnetism and Structure in Chains of Copper Dinuclear Paddlewheel Units

Mireille Perec,*,† Ricardo Baggio,‡ Rosana P. Sartoris,§ Ricardo C. Santana,∥ Octavio Peña,⊥ and Rafael Calvo*,§

†*INQUIMAE−DQIAQF, Facultad de Ciencias Exactas y Naturales, Universidad de Buenos Aires, Ciudad Universitaria, C1428EHA, Buenos Aires, Argentina,* ‡*Comisión Nacional de Energía Atómica, Av. Gral. Paz 1499, 1650 San Martín, Buenos Aires, Argentina,* §*Facultad de Bioquímica y Ciencias Biológicas, Universidad Nacional del Litoral, and INTEC (CONICET−UNL), Güemes 3450, 3000 Santa Fe, Argentina,* ∥*Instituto de Física, Universidade Federal de Goiás, Campus Samambaia, CP 131, 74001−970 Goiânia (GO), Brazil, and* ⊥*UMR 6226 CNRS, Sciences Chimiques de Rennes, Université de Rennes 1, 35042 Rennes, France*

Received October 9, 2009

An anhydrous copper carboxylate compound of formula [Cu(*trans*-2-butenoate)$_2$]$_n$ has been characterized. X-ray analysis reveals a structure built by paddlewheel units bridged by pairs of Cu···O axial bonds to give infinite chains arranged in a new topological motif. Susceptibility measurements in the 10−300 K temperature range, and isothermal magnetization curves at 2, 5, 10, and 50 K with fields up to 5 T, were obtained. Electron Paramagnetic Resonance (EPR) spectra of powder samples were measured at 33.9 GHz at 300 K, and at 9.60 GHz at temperatures in the range 90 ≤ T ≤ 350 K. Fitting the susceptibility data to a chain model of alternating paddlewheel and [Cu(μ-O)$_2$Cu] dinuclear units yielded exchange interactions J_1 = −330.6(1) cm^{-1} and J_2 = 5.9(2) cm^{-1}. The EPR spectra reflect the usual antiferromagnetic dinuclear behavior, with zero field splitting parameters of the excited spin triplet, D = −0.329(3) cm^{-1} and $E \sim 0$, plus a central peak not expected for isolated dinuclear units. We interpret this peak as arising from the stochastic spin dynamics of the chain introduced by exchange couplings between spins in neighbor dinuclear units, which averages out the zero field splitting. Interactions of the units with the rest of the chain acting as a spin bath give rise to a quantum transition between localized dinuclear states and states of the spin chain. This effect competes with the condensation of the antiferromagnetic dinuclear units into the singlet ground state, producing a characteristic temperature dependence of the shape of the powder EPR spectra. We interpret these features in terms of basic theories of magnetic resonance in coupled spin systems applied to the chain array of dinuclear units.

Introduction

Unligated dicopper^{II} tetracarboxylates [Cu$_2$(μ-OOCR)$_4$]$_n$ exhibit chain structures with axial interdimer interactions of copper^{II} centers with carboxylate oxygen atoms of neighboring units. Within this common motif, different structural topologies and connectivities have been reported,[1−14] as well as magnetic and electron paramagnetic resonance (EPR) studies.[14−20]

In previous investigations we reported the synthesis, structure, chemical and magnetic characterization of Cu^{II} and

*To whom correspondence should be addressed. E-mail: perec@qi.fcen.uba.ar (M.P.), calvo@fbcb.unl.edu.ar (R.C.).

(1) Martin, R. L.; Waterman, H. *J. Chem. Soc.* **1957**, 2545–2551.
(2) Simonov, Yu. A.; Malinovskii, T. I. *Sov. Phys. Crystallogr* **1970**, *15*, 310–311.
(3) Bird, M. J.; Lomer, T. R. *Acta Crystallogr., Sect. B: Struct. Sci.* **1972**, *28*, 242–246.
(4) Lomer, T. R.; Perera, K. *Acta Crystallogr., Sect. B: Struct. Sci.* **1974**, *30*, 2912–2913. *Acta Crystallogr., Sect. B: Struct. Sci.* **1974**, *30*, 2913−2915.
(5) Smith, G.; O′Relly, E. J.; Kennard, C. H. L.; White, A. H. *J. Chem. Soc., Dalton Trans.* **1985**, 243–251.
(6) Campbell, G. C.; Haw, J. F. *Inorg. Chem.* **1988**, *27*, 3706–3709.
(7) Troyanov, S. I.; Il′ina, E. G.; Dunaeva, K. M. *Koord. Khim.* **1991**, *17*, 1692–1697.
(8) Il′ina, E. G.; Troyanov, S. I.; Dunaeva, K. M. *Koord. Khim.* **1992**, *18*, 882–892.
(9) Ghermani, N. E.; Lecomte, C.; Rapin, C.; Steinmetz, P.; Steinmetz, J.; Malaman, B. *Acta Crystallogr., Sect. B: Struct. Sci.* **1994**, *50*, 157–160.
(10) Agterberg, F. P. W.; Provo Kluit, H. A. J.; Driessen, W. L.; Oevering, H.; Buijs, W.; Lakin, M. T.; Spek, A. L.; Reedjik, J. *Inorg. Chem.* **1997**, *36*, 4321–4328.
(11) Zubkowski, J. D.; Washington, D.; Njoroge, N.; Valente, E. J.; Cannon, T.; Parks, C. D.; Berdahl, P.; Perry, D. L. *Polyhedron* **1997**, *16*, 2341–2351.
(12) Doyle, A.; Felcman, J.; Gambardella, M. T. D.; Verani, C. N.; Tristao, M. L. B. *Polyhedron* **2000**, *19*, 2621–2627.
(13) Aakeröy, C. B.; Beatty, A. M.; Desper, J.; O'Shea, M.; Valdés−Martínez, J. *Dalton Trans.* **2003**, 3956–3962.
(14) Chung, Y. H.; Wei, H. H.; Liu, Y. H.; Lee, G. H.; Wang, Y. *Polyhedron* **1998**, *17*, 449–455.
(15) Chasteen, D. *Inorg. Chem.* **1971**, *10*, 2339–2340.
(16) Mroziński, J.; Heyduk, E. *J. Coord. Chem.* **1984**, *13*, 291–298.
(17) Campbell, G. C.; Reibenspies, J. H.; Haw, J. F. *Inorg. Chem.* **1991**, *30*, 171–176.
(18) Valko, M.; Mazúr, M.; Morris, H.; Klement, R.; Williams, C. J.; Melník, M. *J. Coord. Chem.* **2000**, *52*, 129–138.
(19) Kozlevčar, B.; Leban, I.; Petric, M.; Petricek, S.; Roubeau, O.; Reedijk, J.; Šegedin, P. *Inorg. Chim. Acta* **2004**, *357*, 4220–4230.
(20) Kozlevčar, B.; Šegedin, P. *Croat. Chem. Acta* **2008**, *81*, 369–379.

Published on Web 12/15/2009

mixed Cu^{II}/Ln^{III} *trans*-2-butenoate compounds.[21−24] In compound $[Cu_2(L)_4(DMF)_2]$ (HL = *trans*-2-butenoic acid) magnetically isolated antiferromagnetic Cu_2 paddlewheel units were studied, and magnetic parameters calculated from magnetic and EPR measurements.[21] Similar results were obtained for $[Cu_2Y_2(L)_{10}(H_2O)_4\cdot 3H_2O]_n$, where copper and yttrium dinuclear units alternate along the chains,[23] in which the Cu_2 paddlewheels are magnetically isolated by diamagnetic Y_2 dinuclear units. During the synthesis of the Cu^{II}/Ln^{III} series with *trans*-2-butenoic acid, a compound was frequently isolated as an amorphous insoluble byproduct. We now succeeded in growing suitable single crystals of this compound as an anhydrous polymer, $[Cu_2(trans\text{-}2\text{-butenoate})_4]_n$, **1**, built on paddlewheel units self-catenated by Cu···O axial bonds into infinite chains in a novel topological motif.

Powder EPR studies reported for unligated Cu^{II} tetracarboxylate polymers were found to display poorly resolved central bands superimposed on the classical signals typical of antiferromagnetically coupled dinuclear copper(II) centers. The central bands disappear from the spectra by decreasing the temperature to ∼100 K. It has been suggested that this may have a correlation with interdinuclear interactions,[16,18−20] but an appropriate theoretical model for this phenomenon is not yet available.

Low dimensional magnetic compounds, mainly one-dimensional (1D), allow the interpretation of experimental information with simple models, calculating the basic interaction parameters without major approximations, and predicting quantum effects.[25−31] The magnetic behavior of chain compounds with equal exchange couplings between each spin and its two neighbors (uniform chains) have been analyzed,[26−28] as well as more complex chains with alternating interactions.[32,33]

Magnetic measurements in **1** allowed evaluating the interactions within the units, and between copper ions in neighbor units in the chain. The powder EPR spectrum displays a broad central peak added to the classical copper(II) acetate signals, as reported for unligated copper carboxylate complexes. We describe herein, a detailed EPR study at 33.9 and 9.6 GHz of a powder sample of **1**, examining the changes of the spectra with temperature. An analysis of the results, based on general magnetic resonance concepts, allows a detailed interpretation of the phenomenon observed in **1** and in previously reported unligated copper(II) carboxylate chains.

Experimental Section

Materials. All reagents were commercially available chemicals of analytical- or reagent-grade purity and used as received. Water was purified by a Millipore milli-Q system, yielding a resistivity of 18 MΩ cm^{-1}.

Synthesis of $[C_8H_{10}CuO_4]_n$, 1. Freshly prepared $Cu(OH)_2$ (1 g, 10 mmol) was mixed with *trans*-2-butenoic acid (2.0 g, 22 mmol) dissolved in 50 mL of water−ethanol (v/v, 1:1) at room temperature, under stirring. A green−blue powder was collected, washed with small amounts of ethanol, and dried in air. Yield: ∼85% based on copper hydroxide. The material is sparingly soluble in most common polar and non-polar solvents. Recrystallization from a very dilute solution in ethanol afforded, after several months, few well-shaped green crystals suitable for structural characterization. Elemental analyses (EA) of C and H were performed on a Carlo Erba 1108 elemental analyzer. Copper content was determined on a Shimadzu AA6501 spectrophotometer. Anal. Calcd. for $C_8H_{10}CuO_4$: C, 41.1; H, 4.3; Cu, 27.2. Found: C, 41.0; H, 4.2; Cu, 27.0%. The compound was identified as Cu(*trans*-2-butenoate)$_2$ by EA, IR, and X-ray powder diffraction (see S1 in ref 23). Infrared spectra were recorded as KBr pellets and as Nujol mulls on a Nicolet 510P FT−IR spectrophotometer. Main bands (KBr disk, ν/cm^{-1}): 1650(m,vbr), 1509(vs, $\nu(CO_2^-)$asym), 1430 and 1394(vs, $\nu(CO_2^-)$sym), 1098 (m), 1051(s), 878(s,vbr), 818(s), 751(m), 712(m), 574((w), 524(m), 504(m), 428(w). Thermogravimetric measurements were carried out using a Shimadzu DTG 50 thermal analyzer under an airflow of 40 L/min at a heating rate of 5 °C min^{-1}. Decomposition occurs in one step in a narrow temperature (T) range centered at 299 °C. The final residual mass of about 35% suggests the formation of CuO, as confirmed by X-ray diffraction (XRD).

X-ray Crystallography. Single crystal. XRD data were collected on a Bruker AXS SMART APEX CCD diffractometer using monochromatic Mo Kα radiation (λ = 0.71069 Å). We used the programs SMART[34] and SAINT[35] as the driving and data integration software. Semiempirical absorption corrections were applied using SADABS.[36] The structure was solved by direct and difference Fourier methods and refined by least-squares on F^2 with anisotropic displacement parameters for non-H atoms. Hydrogen atoms defined by the stereochemistry were placed at their calculated positions and allowed to ride onto their host carbons both in coordinates as well as in thermal parameters. Those corresponding to water molecules, not found in the final difference Fourier maps, were accordingly disregarded in the model. All calculations to solve the structures, refine the models, and obtain derived results were carried out with the computer programs SHELXS97, SHELXL97,[37] and SHELXTL.[38] Full use of the CCDC package was made for searching in the CSD Database.[39] The crystallographic data (excluding structure factors) reported in this paper have been deposited with the Cambridge Crystallographic Data Centre as Supporting Information, CCDC number: 747740. Copies of the data can be obtained free of charge upon application to CCDC, 12 Union Road, Cambridge CB2 1EZ, United Kingdom (Fax: (44) 1223 336−033; e-mail: deposit@ccdc.cam.ac.uk).

(21) Schlam, R. F.; Perec, M.; Calvo, R.; Lezama, L.; Insausti, M.; Rojo, T.; Foxman, B. M. *Inorg. Chim. Acta* **2000**, *310*, 81–88. The value of the intradinuclear exchange interaction calculated from the susceptibility data reported in this work is $J = (-306 \pm 1)$ cm^{-1}.
(22) Barja, B.; Baggio, R.; Garland, M. T.; Aramendia, P. F.; Peña, O.; Perec, M. *Inorg. Chim. Acta* **2003**, *346*, 187–196.
(23) Calvo, R.; Rapp, R. E.; Chagas, E.; Sartoris, R. P.; Baggio, R.; Garland, M. T.; Perec, M. *Inorg. Chem.* **2008**, *47*, 10389–10397.
(24) Calvo, R.; Rapp, R. E.; Sartoris, R. P.; Santana, R. C.; Perec, M. *J. Phys. Chem. A* **2009**, *113*, 8830–8833.
(25) de Jongh, L. J.; Miedema, A. R. *Adv. Phys.* **1974**, *23*, 1–260.
(26) Griffiths, R. G. *Phys. Rev.* **1964**, *133*, A768–775.
(27) Bonner, J.; Fisher, M. *Phys. Rev.* **1964**, *135*, A640–658.
(28) Griffiths, R. G. *Phys. Rev.* **1964**, *135*, A659–660.
(29) Okuda, K.; Hata, H.; Date, M. *J. Phys. Soc. Jpn.* **1972**, *33*, 1574–1580.
(30) Kahn, O. *Molecular Magnetism*; Wiley VCH: New York, 1993.
(31) Georges, R.; Borrás−Almenar, J. J.; Coronado, E.; Curély, J.; Drillon, M. In *Magnetism: Molecules to Materials. Model and Experiments*; Miller, J. S., Drillon, M., Eds.; Wiley−VCH: New York, 2001; pp 1−47.
(32) Duffy, W.; Barr, K. P. *Phys. Rev.* **1968**, *165*, 647–654.
(33) Johnston, D. C.; Kremer, R. K.; Troyer, M.; Wang, X.; Klümper, A.; Bud'ko, S. L.; Panchula, A. F.; Canfield, P. C. *Phys. Rev B* **2000**, *61*, 9558–9606.
(34) *SMART-NT*, V5.624; Siemens Analytical X-ray Instruments Inc.: Madison, WI, 2001.
(35) *SAINT-NT*, V6.22; Siemens Analytical X-ray Instruments Inc.: Madison, WI, 2001.
(36) Sheldrick, G. M. *SADABS*; Bruker AXS Inc.: Madison, WI, 2002.
(37) Sheldrick, G. M. *SHELXS 97; SHELXL 97*; University of Göttingen: Göttingen, Germany, 1997.
(38) *SHELXTL-NT*; Bruker AXS Inc.: Madison, WI, 2001.
(39) Allen, F. H. *Acta Crystallogr., Sect. B: Struct. Sci.* **2002**, *58*, 380–388.

Table 1. Selected Single-Crystal XRD Data for **1**

formula	C_8H_{10} Cu O_4
Fw	233.70
cryst syst	triclinic
space group	$P\bar{1}$
a (Å)	10.3488(7)
b (Å)	10.3719(7)
c (Å)	14.7370(9)
α (deg)	108.0100(10)
β (deg)	103.4650(10)
γ (deg)	90.6540(10)
V (Å^3)	1457.00(17)
Z	6
ρ_{calcd}, g cm^{-3}	1.598
μ /mm^{-1}	2.227
$F(000)$	714
T, K	297(2)
crystal size/mm^3	0.22 × 0.14 × 0.08
θ range, deg.	1.50 to 27.93
index ranges	
	$-12 \le h \le 12$
	$-13 \le k \le 13$
	$-19 \le l \le 19$
reflns (collected, independent, $[I > 2\sigma_{(I)}]$	12161, 6200(0.0293), 4259
max and min transmission	0.84 and 0.70
GOF on F^2	1.013
final R indices $[I > 2\sigma_{(I)}]$	R1[a] = 0.0559
	wR2[b] = 0.1212
R indices (all data)	R1[a] = 0.0879
	wR2[b] = 0.1403
diff. peak, hole	1.013, −0.603 (e Å^{-3})

[a] R1: $\sum||F_o| - |F_c||/\sum|F_o|$. [b] wR2: $\{\sum w(F_o^2 - F_c^2)^2/\sum w(F_o^2)^2\}^{1/2}$.

Magnetic Measurements. Magnetic measurements were performed on a sample containing 41.6 mg of finely powdered material packed in a Teflon film sample holder, having small diamagnetic contribution with a Quantum Design Squid magnetometer model MPMS XL5. The magnetic susceptibility was measured in the temperature interval $10 < T < 300$ K, with an applied magnetic field $B_0 = \mu_0 H = 200$ mT (μ_0 is the permeability of the vacuum). Magnetization measurements were performed at 2, 5, 10, and 50 K, with B_0 between 0 and 5 T. Because of the strong antiferromagnetic interactions within the dicopper tetra-carboxylate units, the magnetic response of the compound at low T is very weak, and the relatively important diamagnetic and temperature independent contributions of the sample and sample holder were evaluated from the isothermal magnetization curve at 50 K. The isothermal magnetization curves at 2 and 5 K, and the susceptibility data below 50 K were assigned to traces of paramagnetic mononuclear impurities.

EPR Spectra. Spectra of fine powdered samples of **1** were collected with Bruker ER−300 and ESP−300E spectrometers working at 33.9 GHz (at 300 K) and 9.60 GHz (as a function of T between 90 and 350 K), using cavities with 100 kHz field modulation and an Eurotherm temperature controller system. A small quantity of MgO doped with Cr^{III} within the cavity was used as a g-marker ($g = 1.9797$). The spectra were analyzed using EasySpin,[40] an EPR simulation package working under Matlab.[41] Some features of this package were also used to evaluate the magnetic properties.

Results and Discussion

Crystal Structure. Crystallographic data of $[Cu_2(O_2CCHCHCH_3)_4]_n$ are given in Table 1, and selected bond distances and angles in Table 2. There are three crystallographically distinct copper^{II} sites with almost ideal

Table 2. Selected Bond Distances (Å) and Angles (deg) for **1**[a]

Cu1−O14	1.939(3)	Cu1−O11	1.942(3)
Cu1−O12	1.959(3)	Cu1−O23	1.994(3)
Cu1−O26′	2.221(3)	Cu2−O24	1.938(3)
Cu2−O21	1.941(3)	Cu2−O13	1.963(3)
Cu2−O22	2.006(3)	Cu2−O22″	2.207(3)
Cu3−O25′	1.932(3)	Cu3−O15	1.944(3)
Cu3−O16	1.957(3)	Cu3−O26′	2.011(3)
Cu3−O23	2.197(3)		
Cu1−Cu2	2.5765(8)	Cu3−Cu3′	2.5844(11)
Cu1−Cu3	3.2458(8)	Cu2−Cu2′	3.2262(11)
O14−Cu1−O11	89.51(15)	O14−Cu1−O12	169.55(13)
O11−Cu1−O12	89.23(15)	O14−Cu1−O23	90.16(14)
O11−Cu1−O23	170.27(13)	O12−Cu1−O23	89.33(14)
O14−Cu1−O26′	90.35(12)	O11−Cu1−O26′	110.56(13)
O12−Cu1−O26′	99.80(12)	O23−Cu1−O26′	79.17(11)
O24−Cu2−O21	88.94(16)	O24−Cu2−O13	90.48(15)
O21−Cu2−O13	169.35(14)	O24−Cu2−O22	170.13(13)
O21−Cu2−O22	89.81(14)	O13−Cu2−O22	88.95(14)
O24−Cu2−O22″	109.73(13)	O21−Cu2−O22″	97.41(13)
O13−Cu2−O22″	92.79(12)	O22−Cu2−O22″	80.14(12)
O25′−Cu3−O15	169.49(14)	O25′−Cu3−O16	88.92(15)
O15−Cu3−O16	89.35(15)	O25′−Cu3−O26′	91.45(14)
O15−Cu3−O26′	88.37(14)	O16−Cu3−O26′	169.43(12)
O25′−Cu3−O23	94.04(14)	O15−Cu3−O23	96.25(14)
O16−Cu3−O23	111.13(12)	O26′−Cu3−O23	79.38(11)

[a] Symmetry transformations used to generate equivalent atoms: ′, $-x+1, -y+1, -z+1$; ″, $-x+1, -y+1, -z$.

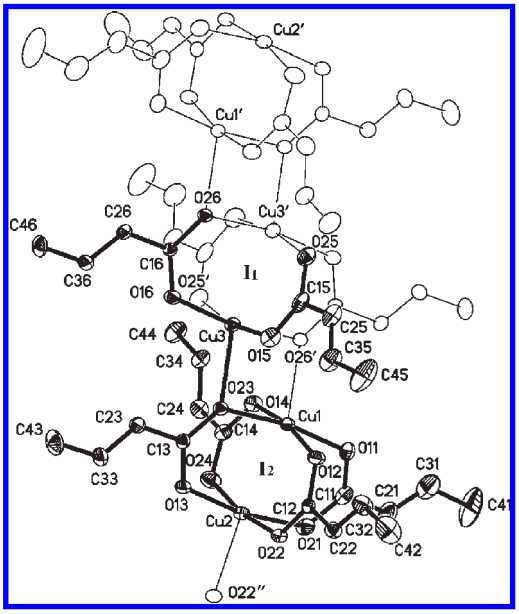

Figure 1. Ellipsoid plot for **1**, showing in bold, full (40% probability level) displacement ellipsoids the asymmetric unit. Symmetry transformations used to generate equivalent atoms: ′, $-x+1, -y+1, -z+1$; ″, $-x+1, -y+1, -z$.

$Cu^{II}O_5$ square pyramidal coordination polyhedral, as expressed by Addison's[42] τ ($\tau < 0.01$) formed by the carboxylate oxygens of three μ_2 bidentate and three μ_3 tridentate carboxylate groups, (trailing numbers 2, 3, 4 and 1, 5, 6, in Figure 1). These secondary building units (SBUs) self-associated by pairs of Cu···O intermolecular axial contacts, give rise to paddlewheel units I_1 and I_2 which differ in their crystallographic symmetry: I_1 being

(40) Stoll, S. *Int. EPR Soc. Newsletter* **2003**, *13*, 24–26. Stoll, S.; Schweiger, A. *J. Magn. Reson.* **2006**, *178*, 42–55.
(41) *Matlab*, The Mathworks Inc.: Natick, MA.
(42) Addison, A. W.; Rao, T. N.; Reedijk, J.; van Rijn, J.; Verschoor, G. C. *J. Chem. Soc., Dalton Trans.* **1984**, 1349–1356.

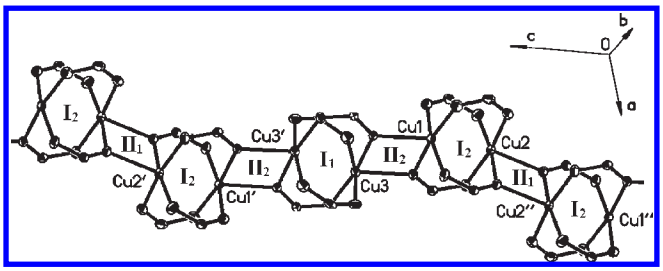

Figure 2. Perspective view of **1** presenting the way in which pairs of paddlewheel units self-bind into chains, giving rise to a stepped polymeric structure along *c*. Symmetry codes as in Figure 1.

Table 3. $\pi\cdots\pi$ Interactions between Pairs of C=C Bonds

pair 1	pair 2	angle (deg)	intercentroid distance (Å)	slippage angle (deg)
C21=C31	(C23=C33)^{i}	171.1(1)	3.775(1)	4.4(3.)
C25=C35	(C25=C35)^{ii}	180	3.948(1)	30.(1)
C26=C36	(C26=C36)^{iii}	180	3.582(1)	0.5(1)

^{i} Symmetry code: x, $1+y$, z. ^{ii} Symmetry code: $2-x$, $1-y$, $1-z$. ^{iii} Symmetry code: $1-x$, $-y$, $1-z$.

strictly centrosymmetric while I_2 is not. Figure 2 depicts the way in which these paddlewheels develop into a stepped polymeric structure along *c* with almost perfectly perpendicular planes (90.0 ± 1.1)° in I_1 and (90.0 ± 1.9)° in I_2, and differing in their mutual orientation in less than 10°.

The Cu···Cu distances in the 4-fold bridged I_1 and I_2 units are, respectively, 2.584(1) Å and 2.576(1) Å. Independent Cu^{II} centers have four oxygen atoms in equatorial sites, with Cu···O distances in the range 1.932−1.994 Å, and Cu···O distances in the apexes in the range 2.197(3)−2.221(3) Å. As a result, two crystallographically different CuO_2Cu binding motifs involving the axial copper bonds are formed (II_1 and II_2 in Figure 2), almost at right angles to each other, II_1 being strictly centrosymmetric and II_2 only nearly so. The Cu···Cu distances are 3.226(1) Å in II_1 and 3.246(1) Å in II_2. The chains, running along *c* at average axis-to-axis separation of 10.35 Å, are quite independent; they only interact with each other through weak $\pi\cdots\pi$ interactions involving the C2x = C3x double bonds of neighboring *trans*-2-butenoate ligands. These secondary interactions connect chains along the *a* and *b* directions and are the main stabilizing agents for the network (Table 3). There are, in addition, three relevant weak intra-chain H-bonding interactions involving the C(sp^2)-H groups (trailing numbers 2,3 and 6 in Figure 1) and carboxylate oxygens with C−H···O angles larger than 150°, which contribute to link the chains along the *c* direction. The common feature in these packing motifs is the repetition pattern of the CuO_2Cu bridging units, which can appear along the resulting chains in any of two almost perpendicular orientations, Figure 3. Different chain types have been reported for similar Cu^{II} carboxylates according to the orientations of these loops and their sequence along the chains. A search in the CCD reveals that for copper chains the packing pattern known as *flat ribbon*, (1) in Figure 3, predominates, with 14 occurrences out of a total of 16. In this type, neighboring bridging loops are parallel

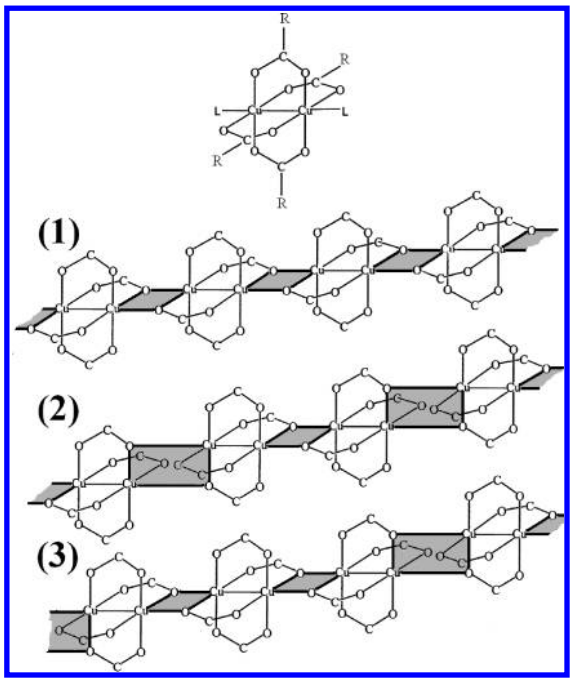

Figure 3. Illustration of various 1D packing patterns resulting from the self-assembly of paddlewheel units.

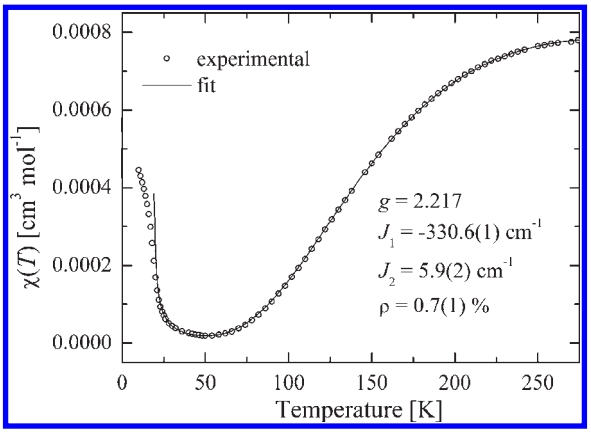

Figure 4. Molar magnetic susceptibility of **1** as a function of temperature measured at B_0 = 200 mT. Symbols are corrected experimental results. The solid line represents the best fit for a model with 5 dinuclear units to the data.

to each other and link to opposite "hemispheres" of the central paddlewheel. Two less favored sequences, having perpendicular O-bridges as type (2) in Figure 3, were reported in $[Cu_2(C_5H_{11}O_2Si)_4]_n$, and $[Cu_2(O_2CCF_3)_4]_n$.[43−45] The structure presented herein displays a new, so far unreported motif (type 3 in Figure 3) that is composed of two consecutive loops parallel to each other (II_2 in Figure 2) and a third one (II_1 in Figure 2), perpendicular to both.

Magnetic Properties. Figure 4 displays the *T* variation of the magnetic susceptibility $\chi(T)$ of **1** measured at B_0 = 200 mT and calculated per mol of $C_8H_{10}CuO_4$.

(43) Nakagawa, H.; Kani, Y.; Tsuchimoto, M.; Ohba, S.; Matsushima, H.; Tokii, T. *Acta Crystallogr., Sect. C: Cryst. Struct. Commun.* **2000**, *56*, 12–16.
(44) Karpova, E. V.; Boltalin, A. I.; Korenev, Yu. M.; Troyanov, S. I. *Koord. Khim.* (*Russ.*)(*Coord. Chem.*) **2000**, *26*, 361–366.
(45) Cotton, F. A.; Dikarev, E. V.; Petrukhina, M. A. *Inorg. Chem.* **2000**, *39*, 6072–6079.

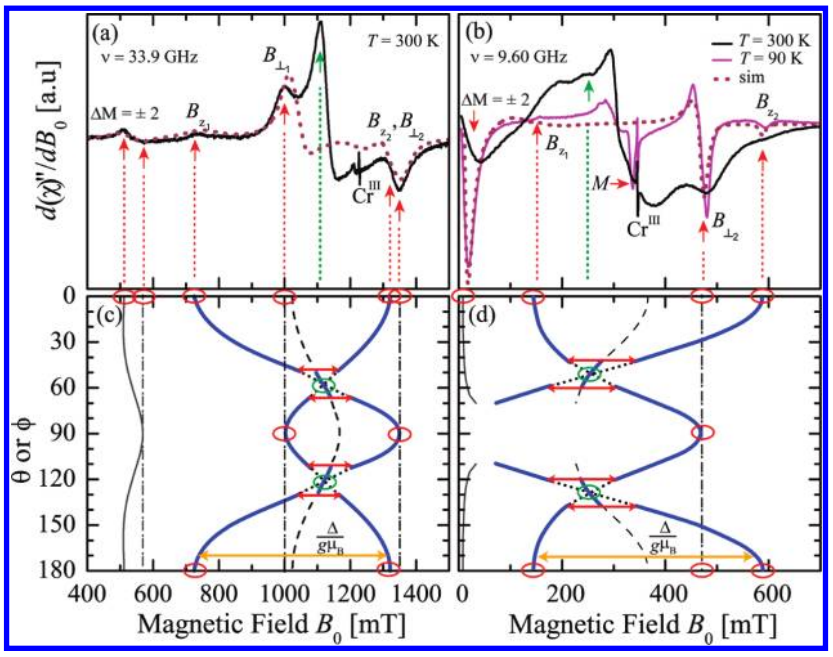

Figure 5. EPR spectra of a powder sample of **1** at, (a) 33.9 GHz and 300 K; (b) 9.60 GHz, at 90 and 300 K, normalized to the same peak-to-peak span. Solid lines are experimental results and dotted lines are simulations performed with the parameters given in the text. (c) and (d) display the angular variations of the positions of the resonances calculated with the parameters given in the text at each microwave frequency. The dotted red arrows in (a) and (b) correlate the positions of the dinuclear peaks of the spectra (labeled with the standard nomenclature) with the angular variation of the lines (see red ovals in (c) and (d)). To explain the origin of the central peak we indicate with green ovals in (c) and (d) the crossing of the $\pm 1 \leftrightarrow 0$ transitions in the *zx* or *zy* planes. The red arrowed lines around these ovals separate angular regions where split or merged resonances occur. The dotted green arrow relate the merging process described in (c) and (d) with the central peak of the spectrum.

Isothermal magnetization $M(B_0,T)$ at 2, 5, 10, and 50 K with fields B_0 between 0 and 5 T having magnitudes much smaller than those expected for paramagnetic Cu^{II} at the same B_0 and T are shown in the Supporting Information, Figure S1 (solid symbols). Since $M(B_0,T)$ at T = 2 and 5 K and high magnetic fields display some degree of saturation not expected for strongly coupled AFM units, the low T behavior of $\chi(T)$ and $M(B_0,T)$ can be attributed to traces (less than 1%) of paramagnetic copper. The paramagnetic contribution to the magnetic moment $m(B_0,T)$ of the sample plus sample holder observed at 50 K (Supporting Information, Figure S2) is small and displays linear field dependence with a negative slope which is used to correct the susceptibility data in Figure 4 for contributions independent of T. With these corrections incorporated, $\chi(T)$ is nearly zero at 50 K, and above that temperature it displays a T dependence typical for strongly coupled AFM dinuclear units, Figure 4. Below 50 K, it increases with decreasing T, as expected from the presence of traces of mononuclear paramagnetic impurities.[30] The magnetization data at 50 K is also used to correct the magnetization curves at lower T from temperature independent correction (empty symbols in Supporting Information, Figure S1).

EPR Spectra. The powder EPR spectra ($d\chi''/dB_0$) at 33.9 GHz (300 K) and 9.60 GHz (300 and 90 K) are displayed in Figures 5a and 5b, respectively. The peaks B_{z_1}, B_{z_2}, $B_{\perp_1}$, and $B_{\perp_2}$ are assigned and labeled according to the standard notation for dinuclear units with approximate axial symmetry.[46−48] We also assign the double quantum transition ($\Delta M = \pm 2$) at low field. All spectra are normalized to the same peak-to-peak span and show the narrow peak corresponding to the paramagnetic Cr^{III} marker. The additional intense and wide central peaks with B_0 = 1110 mT and B_0 = 244 mT appearing at 33.9 and 9.60 GHz, respectively, are reproducible in independent preparations and too strong to be attributed to contamination with paramagnetic mononuclear spins. To investigate their origin we measured the temperature dependence of the spectra between 90 and 350 K at 9.60 GHz, Figure 6. The central peak decreases in relative intensity with decreasing T and disappears at low T, a behavior different from that normally attributed to traces of mononuclear Cu^{II}, expected to increase the relative intensity with decreasing T. This T dependence discards the normally invoked assignment to mononuclear paramagnetic impurities,[30] that in our case may only be responsible of a small residual signal, which can be traced to the increase of the susceptibility below 50 K in Figure 4, observed at the lowest temperatures (labeled M in Figures 5b and 6). The peaks corresponding to the dinuclear unit broaden and tend to disappear with increasing T, when the central transition assigned to the spin chain becomes dominant, Figure 6. To complete the analysis of the temperature variation of the spectra of **1**, we analyzed the variation with T of the relative intensity of the central peak. The open circles in Figure 7 display T multiplied by the relative intensity ratio R between the

(46) Wasserman, E.; Snyder, L. C.; Yager, W. A. *J. Chem. Phys.* **1964**, *41*, 1763–1772.
(47) Bencini, A.; Gatteschi, D. *Electron Paramagnetic Resonance of Exchange Coupled Systems*; Springer: Berlin, 1990.
(48) Weil, J. A.; Bolton, J. R.; Wertz, J. E. *Electron Paramagnetic Resonance. Elementary Theory and Practical Applications*; Wiley: New York, 1994.

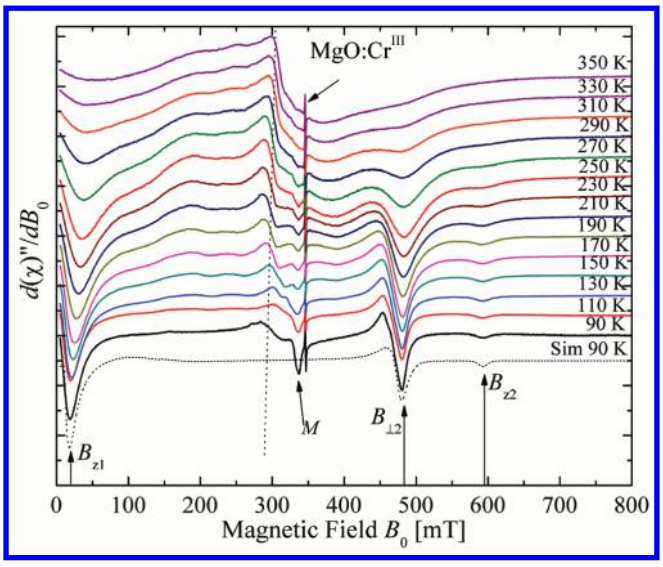

Figure 6. EPR spectra of a powder sample of **1** observed at 9.60 GHz as a function of temperature. The spectra are normalized to the same peak-to-peak span. Dotted line is a simulation with the parameters given in the text of the spectrum at 90 K. The dinuclear moiety peaks B_{z_1}, B_{z_2}, and $B_{\perp_2}$ and that due to traces of mononuclear impurities (M) are indicated. The vertical dashed line emphasizes the narrowing of the central line with decreasing T.

areas of the peak $B_{\perp_2}$, corresponding to the dinuclear unit and that of the signal corresponding to the Cr^{III} marker.

Modeling and Discussion of the Data

Magnetic Properties. We modeled the magnetic properties of **1** considering alternating spin chains containing $2n$ Cu^{II} ions with equal couplings J_1 within the n paddlewheel units I_1 or I_2,[30,49] and also equal couplings J_2 supported by the bridges II_1 and II_2. Since the magnetic measurements were performed in powder samples, we assumed equal angular-averaged g-factors for all Cu^{II} ions. In the presence of a magnetic field $\boldsymbol{B_0}$ we considered the Hamiltonian:

$$\mathscr{H} = \sum_{i=1}^{n} g\mu_B(\mathbf{S}_{2i-1} + \mathbf{S}_{2i})\cdot\boldsymbol{B}_0 - \sum_{i=1}^{n}[J_1\mathbf{S}_{2i}\cdot\mathbf{S}_{2i-1} + J_2\mathbf{S}_{2i}\cdot\mathbf{S}_{2i+1}] \quad (1)$$

where $\mathbf{S}_k$ are spin operators ($S = 1/2$) corresponding to Cu^{II} ions in the **k** position of the chain, and we use a periodic condition for a spin ring, $\mathbf{S_1} = \mathbf{S_{2n+1}}$. The method used to calculate the magnetic properties for finite alternate spins 1/2 chains follows that introduced by Bonner and Fisher[27] and modified by Duffy and Barr.[32] The matrix elements of $\mathscr{H}$ for closed chains (rings) were calculated using EasySpin,[40] the eigenvalues were obtained by numerical diagonalization, and the molar susceptibility $\chi(T)$ and magnetization $M(B_0,T)$ were calculated as in refs 27, 50, and 51 for finite chains

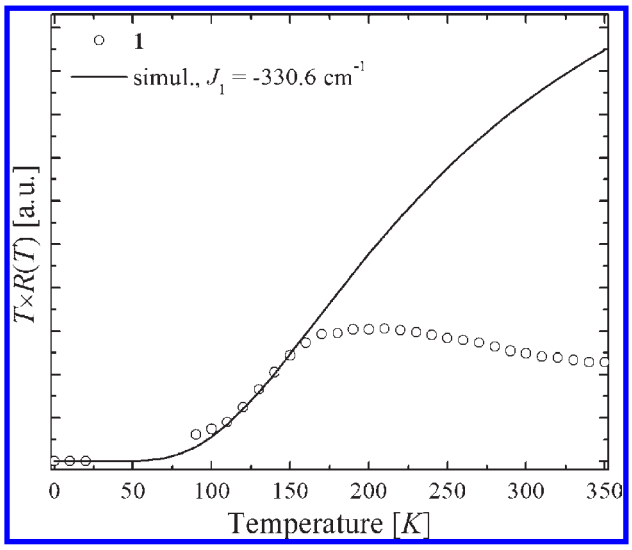

Figure 7. Product T times ratio R between the areas of the signal $B_{\perp 2}$ corresponding to the dinuclear unit and that of the Cr^{III}:MgO paramagnetic marker, as a function of temperature. The solid line is the prediction for independent dinuclear units with $J_1 = -330.6\ cm^{-1}$.

with $n = 2$ to 5 units (10 spins 1/2), as a function of g, J_1, and J_2. Least squares fits of the predictions of the susceptibility for chains with $n = 4$ and 5 units to the data above 50 K yielded $g = 2.217(5)$, $J_1 = -330.6(1)$ cm^{-1}, and $J_2 = 5.9(2)$ cm^{-1}. The relevance of J_2 in the magnetic behavior is reflected by an increase of the standard deviation between the fits and the data of approximately 10% neglecting this coupling. The agreement between experimental and calculated values above 50 K (solid lines in Figure 4) is comparable to the experimental uncertainty. Below that, $\chi(T)$ is dominated by the contribution of mononuclear Cu^{II} impurities, which are not important in our analysis. A fit of this contribution as suggested by Kahn[30] giving a ratio $\rho = 0.7\%$ between the quantities of monatomic and the quantities of dimeric copper ions in the sample, explains adequately the low T behavior (see solid line in Figure 4, where this contribution is considered). This model and values of the parameters were also used to analyze the molar magnetization at 2 and 5 K, Supporting Information, Figure S1; the calculated values of $M(B_0,T)$ are more than 10 times smaller than the data, and its field dependence is linear (unsaturated magnetization), supporting the presence of less than 1% of mononuclear Cu^{II}, as occurs in similar cases.[30] We attempted to fit the susceptibility data considering different couplings within units I_1 and I_2, but improvement of the fit was negligible. Our calculations show that, because of the large difference between $|J_1|$ and $|J_2|$, chains with $n = 4$ or 5 dinuclear units (8 or 10 Cu spins) are long enough for an accurate calculation of magnetic properties.

The coupling $J_1 = -330.6\ cm^{-1}$ between Cu^{II} ions at ~2.58 Å in the paddlewheel units I_1 and I_2 (assumed to be equal) in **1** may be conveniently compared with the value $J_1 = -338\ cm^{-1}$ calculated for $[Cu_2Y_2L_{10}(H_2O)_4\cdot 3(H_2O)]_n$, (HL = *trans*-2-butenoic acid), where similar Cu_2 paddlewheels units alternate with diamagnetic Y_2 dinuclear units.[23]

The calculated ferromagnetic coupling $J_2 = 5.9\ cm^{-1}$ for the CuO_2Cu units can be compared with the couplings

(49) Carlin, R. L. *Magnetochemistry*; Springer: Berlin, 1985.
(50) Costa−Filho, A. J.; Nascimento, O. R.; Ghivelder, L.; Calvo, R. *J. Phys. Chem. B* **2001**, *105*, 5039–5047.
(51) Chagas, E. F.; Rapp, R. E.; Rodrigues, D. E.; Casado, N. M. C.; Calvo, R. *J. Phys. Chem. B* **2007**, *110*, 8052–8063.

$J_2 = 3.2\,cm^{-1}$ and $3.3\,cm^{-1}$ observed in the compounds with similar bridges $[Cu(tda)(phen)]_2$ and $[Cu(oda)(phen)]_2$, respectively.[52,53] A model based on the density functional theory (broken symmetry approximation) proposed for the electronic structures of these two complexes gave[53] $J \sim 5.7\ cm^{-1}$, satisfactorily accounting for the experimental results within the uncertainties.

EPR Spectra. $Cu_2(OOCR)_4$ paddlewheel-units have a non-magnetic ground singlet and an excited triplet state. Ever since the pioneering work of Bleaney and Bowers[54] the spectra resulting from the microwave excitation of the triplet state are well understood for powder and single crystal samples containing non-interacting dinuclear units. Additional peaks in the EPR spectra have been observed for a number of unligated copper carboxylates, all having polymeric structures[16,18−20] but no theoretical explanation was given.

To interpret the EPR results obtained for **1** it is necessary to rationalize the origin and temperature dependence of the shape and intensity of the observed central peak. It has been reported[55] that weak exchange interactions between spins give rise to a spin dynamics capable of collapsing the spectra of ions with different *g*-values in a chain[56] or a layer,[57−59] and also collapsing the fine structure of the excited triplet state of weakly coupled dinuclear units in a three-dimensional (3D) array.[60] These results for systems of infinite interacting spins were explained using the general theories of magnetic resonance of Anderson[61,62] and Kubo and Tomita.[63] Along similar lines we demonstrate later that the central signal of the EPR spectra of **1** is a consequence of the weak connection of the strongly coupled AFM dinuclear units giving rise to the spin chains. A quantum-statistical process is set, where the interactions of each unit with the environment of other units destroy the phase of the wave function producing a transition from an isolated dinuclear unit to an infinite spin chain, modifying notably the EPR spectrum, even when the corresponding changes in the static magnetic properties are small. This interpretation is supported by a recent single crystal EPR study of another dinuclear compound.[60]

To prove this-assumption, we added to $\mathscr{H}$ in eq 1 (a) the anisotropy of the *g*-factor and (b) the anisotropic spin−spin interactions (dipolar + anisotropic exchange) within the paddlewheel units, relevant for the EPR but not for the susceptibility of a powder

$$\mathscr{H} = \sum_{i=1}^{n}[\mu_B(\mathbf{S}_{2i-1}+\mathbf{S}_{2i})\cdot g\cdot \boldsymbol{B}_0 - J_1\mathbf{S}_{2i-1}\cdot\mathbf{S}_{2i}] + \sum_{i=1}^{n}\mathbf{S}_{2i-1}\cdot\boldsymbol{D}\cdot\mathbf{S}_{2i} - \sum_{i=1}^{n}J_2\mathbf{S}_{2i}\cdot\mathbf{S}_{2i+1} = \mathscr{H}_0+\mathscr{H}_1+\mathscr{H}_2 \quad (2)$$

$\mathscr{H}_0$ contains the Zeeman coupling with the field $\boldsymbol{B_0}$ and the intradinuclear exchange interactions, predicting an EPR spectrum with a single resonance having an angular dependent position determined by the *g*-matrix that may be assigned to the spin chain. The isotropic exchange term J_1 produces a level splitting, contributing to a temperature dependence of the intensity, but not to the line shape. The anisotropic spin−spin interaction $\mathscr{H}_1$ (mainly dipole−dipole coupling) splits the resonance, giving rise to the characteristic spectral structure of powder, or single crystal samples, of a dinuclear unit.[46,48] The interactions between spins in neighbor dinuclear units, $\mathscr{H}_2$, commutes with $\mathscr{H}_0$, but not with $\mathscr{H}_1$, thus producing a stochastic modulation of $\mathscr{H}_1$ that changes the above-described spectral structure.[61,64]

First, we treat the spectra of independent dinuclear units neglecting $\mathscr{H}_2$ and assuming only one type of $\boldsymbol{g}$ and $\boldsymbol{D}$ matrices having equal principal axes, an assumption supported by the similar geometry and orientations, and approximate axial symmetry of units I_1 and I_2. We fitted $\mathscr{H}_0 + \mathscr{H}_1$ to the spectra (Figures 5a and 5b at 90 K), neglecting the field range where the central peak appears. Within this simplification the sum over non interacting identical units is irrelevant, and the calculation involving a spin system having four states gives a first approximation for the principal values $g_\parallel$, $g_\perp$, D, and E of the $\boldsymbol{g}$ and $\boldsymbol{D}$ matrices within the triplet state. From the spectra at 33.9 (300 K) and 9.6 GHz (90 K) we obtain, respectively, $g_{Cu}^{\parallel} = 2.365(2)$, $g_{Cu}^{\perp} = 2.036(2)$, $D_{Cu} = -0.329(3)\ cm^{-1}$, $E_{Cu} \sim 0$, and $g_{Cu}^{\parallel} = 2.365(2)$, $g_{Cu}^{\perp} = 2.076(2)$, $D_{Cu} = -0.329(3)\ cm^{-1}$, $E_{Cu} \sim 0$ (see references 46, 48, and 60 for definitions of D and E). The sign of D was taken from that recently determined for a similar structure.[65] The simulations obtained with these values, shown as dashed lines in Figures 5a, 5b, and 6, predict the peaks attributed to dinuclear units of the spectrum at 33.9 GHz with good accuracy, but a poorer agreement is obtained at 9.6 GHz, even at 90 K when the resolution is highest (see Figure 6). Within this model of an isolated dinuclear unit, the simulated spectra are not expected to show the central peak.

In the next step of the calculation, we consider the effects produced by the exchange couplings J_2 within units assembled in a chain. We first simulate the spectra of finite closed rings of 2, 3, and 4 coupled units, using the values of J_1 and J_2 obtained from the magnetic data, and the parameters $g_\parallel$, $g_\perp$, D, and E given above. Simulations of EPR spectra of large spin systems require large

(52) Baggio, R.; Garland, M. T.; Manzur, J.; Peña, O.; Perec, M.; Spodine, E.; Vega, A. *Inorg. Chim. Acta* **1999**, *286*, 74–79.
(53) Baggio, R.; Calvo, R.; Garland, M. T.; Peña, O.; Perec, M.; Slep, L. D. *Inorg. Chem. Commun.* **2007**, *10*, 1249–1252.
(54) Bleaney, B.; Bowers, K. D. *Proc. R. Soc., London* **1952**, *214*, 451–465.
(55) Calvo, R. *Appl. Magn. Reson.* **2007**, *31*, 271–299.
(56) Calvo, R.; Levstein, P. R.; Castellano, E. E.; Fabiane, F. M.; Piro, O. E.; Oseroff, S. B. *Inorg. Chem.* **1991**, *30*, 216–220.
(57) Calvo, R.; Mesa, M. A.; Oliva, G.; Zukerman−Schpector, J.; Nascimento, O. R.; Tovar, M.; Arce, R. *J. Chem. Phys.* **1984**, *81*, 4584–4591.
(58) Gennaro, A. M.; Levstein, P. R.; Steren, C. A.; Calvo., R. *Chem. Phys.* **1987**, *111*, 431–438.
(59) Calvo, R.; Passeggi, M. C. G.; Novak, M. A.; Symko, O. G.; Oseroff, S. B.; Nascimento, O. R.; Terrile, M. C. *Phys. Rev. B* **1991**, *43*, 1074–1083.
(60) Napolitano, L. M. B.; Nascimento, O. R.; Cabaleiro, S.; Castro, J.; Calvo, R. *Phys. Rev. B* **2008**, *77*, 214423.
(61) Anderson, P. W.; Weiss, P. R. *Rev. Mod. Phys.* **1953**, *25*, 269–276.
(62) Anderson, P. W. *J. Phys. Soc. Jpn.* **1954**, *9*, 316–339.
(63) Kubo, R.; Tomita, K. *J. Phys. Soc. Jpn.* **1954**, *9*, 888–919.
(64) Pake, G. E. *Paramagnetic Resonance. An Introductory Monograph*; Benjamin: New York, 1962; Chapter 7.
(65) Ozarowski, A. *Inorg. Chem.* **2008**, *47*, 9760–9762.

computer memory and time, impeding calculations for long chains. The spectra of finite chains (not shown) display a number of peaks, increasing in number for higher n, accumulating and overlapping in the central region of the spectrum, thus resembling the experimental observation. Although these simulations approach the observed spectra, they are only a crude approximation to an *infinite* chain of coupled dinuclear units. The EPR spectra of a cluster of spins depends on the spin dynamics which is strongly dependent on its topology and dimension;[66] it is predictable for finite clusters, but stochastic (diffusive) for infinite systems. The problem should be solved for $n \rightarrow \infty$, and the most appropriate approach to this effect is provided by the quantum-statistical theories of magnetic resonance introduced by Anderson[61,62] and Kubo and Tomita,[63] that consider the stochastic spin dynamics of infinite systems (see Pake[64] for a basic description of these theories). Accordingly, the EPR line shape $I(\omega)$ for a spin system described by a Hamiltonian $\mathscr{H}$ is the Fourier transform of the thermal averaged time correlation function $G(t)$ of the magnetization M along the microwave field:

$$I(\omega) = \frac{1}{2\pi}\int_{-\infty}^{\infty} G(t)\mathrm{e}^{-\mathrm{i}\omega t}\,\mathrm{d}t \tag{3}$$

where $G(t)$ is

$$G(t) = \int_{-\infty}^{\infty} I(\omega)\mathrm{e}^{\mathrm{i}\omega t}\,\mathrm{d}t = \frac{\langle M_{\mathrm{x}}(t)M_{\mathrm{x}}(0)\rangle}{\langle M_{\mathrm{x}}(0)M_{\mathrm{x}}(0)\rangle} = \frac{tr[\mathrm{e}^{-\mathscr{H}/k_{\mathrm{B}}T}M_{\mathrm{x}}(t)M_{\mathrm{x}}(0)]}{tr[\mathrm{e}^{-\mathscr{H}/k_{\mathrm{B}}T}M_{\mathrm{x}}(0)M_{\mathrm{x}}(0)]} \tag{4}$$

The symbols $\langle\cdots\rangle$ indicate thermal averages, and $M_x(t)$ is the Heisenberg representation of the time evolution of the magnetization imposed by $\mathscr{H}_2$ of eq 2, containing the interactions of a dinuclear unit with the spin environment (the chain in our case).

$$M_{\mathrm{x}}(t) = \mathrm{e}^{\mathrm{i}\mathscr{H}t/\hbar}M_{\mathrm{x}}\mathrm{e}^{-\mathrm{i}\mathscr{H}t/\hbar} \tag{5}$$

Since $\mathscr{H}$(mainly $\mathscr{H}_0$) involves terms of the order or larger than $k_{\mathrm{B}}T$, high temperature approximations are not valid in eq 4, and T, should be explicitly considered. An equation of motion proposed for $M_x(t)$ in eq 5 is[67−69]

$$\frac{\mathrm{d}M_{\mathrm{x}}(t)}{\mathrm{d}t} = \mathrm{i}\Omega(t)M_{\mathrm{x}}(t) \tag{6}$$

where $\Omega(t)$ in eq 6 is a random frequency function requiring $\langle\Omega(t)\rangle = 0$, associated to the anisotropic spin−spin coupling $\mathscr{H}_1$ (mainly dipolar interaction) giving rise to the spectrum of the dinuclear moieties when it is randomly modulated by the interdinuclear interaction $\mathscr{H}_2$. In a statistical picture, $\Omega(t)$ may be characterized by its second moment Δ and a correlation time τ_{ex}, defined as

$$\Delta = \langle\Omega^2\rangle^{1/2} \quad \text{and} \quad \tau_{\mathrm{ex}} = \frac{2\pi}{\omega_{\mathrm{ex}}} = \int_0^{\infty}\frac{\langle\Omega(t)\Omega(0)\rangle}{\Delta^2}\mathrm{d}t \tag{7}$$

The second moment Δ is related to the projection of the dipolar coupling along $\boldsymbol{B_0}$, whereas τ_{ex} (or the exchange frequency ω_{ex}) is related to the interactions between dinuclear units. When the product $\Delta\tau_{\mathrm{ex}} \gg 1$, the modulation of Ω is slow, and one observes a spectrum similar to that of uncoupled units, with some extra broadening of the peaks. When $\Delta\tau_{\mathrm{ex}} \ll 1$, the modulation is fast, leading to spectra corresponding to chains of copper ions, without fine structure.

Figures 5c and 5d show the angular variations of the fields for the transitions $\pm 1 \leftrightarrow 0$ and $+1 \leftrightarrow -1$ calculated with the spin Hamiltonian parameters given above at 33.9 and 9.60 GHz, for $\boldsymbol{B_0}$ in the planes zx (or zy) and xy of a single crystal sample. The red arrows correlating Figures 5a with 5c, and 5b with 5d, illustrate how the "non interacting dinuclear peaks" of the powder spectra in Figures 5a and 5b arise from the extremes of these angular variations. In Figures 5c and 5d the distance between pairs of lines for each field orientation is the projection of the fine structure coupling along $\boldsymbol{B_0}$, corresponding to Δ of eq 7, in magnetic field units. For species with axial symmetry, Δ varies depending on the orientation in the zx (and zy) planes, but it is constant in the xy plane. The anisotropy of the average position of these pairs of transitions in the zx plane, shown as a dashed line in Figures 5c and 5d, arises from the g-anisotropy. Within the axial symmetry approximation there is no such anisotropy in the xy plane. For each T, τ_{ex} takes a specific value, depending on J_2 and on the average population of the excited triplet state of the units. When $\Delta\tau_{\mathrm{ex}} = 1$, fast and slow modulation regimes can be described, respectively, by the angular ranges separated with the red arrowed lines in Figures 5c and 5d. For $\Delta\tau_{\mathrm{ex}} < 1$ (fast regime), the two lines of the fine structure merge to the average position, and for $\Delta\tau_{\mathrm{ex}} > 1$ the dipole−dipole splitting is observed. The merging of the signals to the average position give rise to the central line indicated by a green arrow in Figures 5a and 5b, which grows and broadens with increasing T as τ_{ex} decreases, and the red line is displaced to larger values of Δ. The broadening of the central peak as a function of T observed in Figure 6 is also rationalized considering the anisotropy of the average position in the zx plane. A powder spectrum, obtained from a sample that contains microcrystals with all field orientations, contains contributions in the slow and fast modulation regime, and thus it displays simultaneously characteristics of isolated dinuclear units and of linear chains. This justifies the fit of the spin Hamiltonian to the dinuclear peaks of the spectra, neglecting the central peak.

Further support of our interpretation is the temperature dependence of the product of temperature times the

(66) Richards, P. M. In *Local Properties at Phase Transitions*; Muller, K. A., Rigamonti, A., Eds.; Editrice Compositori: Bologna, Italy, 1975; p 539.
(67) Kubo, R. In *Fluctuation, Relaxation, and Resonance in Magnetic Systems*; Ter Haar, D., Ed.; Oliver and Boyd: Edinburgh, U.K., 1962; p 23. Kubo, R. In *Stochastic Processes in Chemical Physics*, Schuler, K. E., Ed.; Advances in Chemical Physics; Interscience: New York, 1969; Vol. *15*, p 101.
(68) Kubo, R.; Toda, M.; Hashitsume, N. *Statistical Physics II. Non Equilibrium Statistical Mechanics*; Springer: Berlin, 1978.
(69) Zwanzig, R. *Nonequilibrium Statistical Mechanics*; Oxford University Press: New York, 2001.

ratio between the intensities of the dinuclear signal (Figure 7). The solid line in the figure represents the temperature dependence expected for isolated dinuclear units with $J_1 = -330.6\ cm^{-1}$.[24,60,70] The results at low T follow this line, but at high T the behavior of coupled dinuclear units is different. At low T values, the intensity changes with increasing temperatures because the relative population of the excited triplet state increases. This temperature dependence is directly related to the Bleaney and Bowers equation[24,54,70] which rules the behavior of the magnetic susceptibility of isolated units. However, this explanation does not hold at higher T, when part of the relative growth of the intensity of the dinuclear peaks with T is lost because of the merger of the dinuclear to the central peak. Thus, the solid line calculated for isolated dinuclear units[24] does not hold at high T, and the deviation between the experimental results and this curve is attributed to the coupling J_2.

Conclusions

We have studied the structure and behavior of chains of anhydrous copper carboxylate paddlewheel units bridged by pairs of axial Cu···O bonds showing a previously unknown topological motif.

The EPR results presented here for **1** are most interesting. The observed spectra display a central line strongly dependent on temperature, superimposed to the standard spectrum of the dinuclear unit. This peak, observed in previous powder EPR studies of related carboxylate chains, has not received to date a proper explanation. We report here a detailed analysis supported by a previous investigation in single crystals of dinuclear compounds where it was possible to follow the collapse of the structure of EPR lines produced by the interaction between dinuclear units in a 3D array.[60] The parameter varied in this case was the line splitting Δ as a function of the orientation of the magnetic field, while the coupling between units was kept constant. The procedure allowed determining interactions as small as $0.060\ cm^{-1}$ and a well-defined transition between two states. In the present work, the orientational random distribution of crystallites in the powder provides a distribution of values of Δ within the sample, and we vary the temperature of the sample, which determines the population of the triplet state and, correspondingly, the correlation time τ_{ex} (or exchange frequency ω_{ex}). The experiment is thus simpler, and the range of application is wider. Unfortunately, we have not succeeded yet in obtaining a single crystal appropriate for EPR studies. In addition, the triclinic space symmetry of **1** would introduce difficulties for accurate sample orientation.

Interactions between dinuclear or polynuclear magnetic units contributing to the magnetic relaxation are of interest in molecular magnetism. The couplings and their consequences may be studied in finite supramolecular structures composed of groups of weakly bonded molecules,[71,72] or in infinite interacting systems. Our approach provides a valuable route to detect and estimate these interactions. We express and calculate the wave function, through a range spanned by a localized system, the isolated dinuclear unit in **1**, to an extended one, the spin chain, or eventually a two- or three-dimensional system. Electron paramagnetic resonance, having the possibility of detecting the time response of the magnetization, provides a very appropriate tool for this purpose.

Acknowledgment. The authors acknowledge the ECOS Sud A05E01, France−Argentina Binational Cooperation Project that made possible this collaboration. This work was supported by PIP 5274 from CONICET and PICT 25409 BID/728/OC/AR in Argentina, and by CNPq in Brazil. M.P. and R.C. are members of CONICET.

Supporting Information Available: Additional information as noted in the text. This material is available free of charge via the Internet at http://pubs.acs.org.

(70) Wasson, J. R.; Shyr, C. I.; Trapp, C. *Inorg. Chem.* **1968**, *7*, 469–473.

(71) Wernsdorfer, W.; Aliaga−Alcalde, N.; Hendrickson, D. N.; Christou, G. *Nature* **2002**, *416*, 406–409.

(72) Wernsdorfer, W.; Bhaduri, S.; Tiron, R.; Hendrickson, D. N.; Christou, G. *Phys. Rev. Lett.* **2002**, *89*, 197201.